We are IntechOpen, the world's leading publisher of Open Access books Built by scientists, for scientists

4,800
Open access books available

122,000
International authors and editors

135M
Downloads

Our authors are among the

154
Countries delivered to

TOP 1%
most cited scientists

12.2%
Contributors from top 500 universities

CLARIVATE ANALYTICS BOOK CITATION INDEX INDEXED

WEB OF SCIENCE™

Selection of our books indexed in the Book Citation Index in Web of Science™ Core Collection (BKCI)

Interested in publishing with us?
Contact book.department@intechopen.com

Numbers displayed above are based on latest data collected.
For more information visit www.intechopen.com

Chapter 15

Novel Fischer's Base Analogous of Leuco-TAM and TAM$^+$ Dyes – Synthesis and Spectroscopic Characterization

Sam-Rok Keum, So-Young Ma and Se-Jung Roh

Additional information is available at the end of the chapter

http://dx.doi.org/10.5772/48119

1. Introduction

Triarylmethane (TAM) dyes are organic compounds containing triphenylmethane backbones. TAM compounds are sometimes called leuco-TAMs (LTAMs) or leuco-bases. (Nair et al., 2006) LTAM molecules are the precursors of TAM$^+$ dyes since TAM$^+$ dyes are the oxidized form of LTAM molecules. Backbones of TAM molecules are also known to be an important group in intermediates in the synthesis of various organic functional compounds, including the preparation of polymers and supramolecules. (Bartholome & Klemm, 2006)

TAM$^+$ dyes potentially have numerous applications in the chemical, pharmaceutical, and life science industries, including as staining agents, ink dyes, thermal imaging materials, carbonless copying materials, drugs, leather, ceramics, cotton, and as a cytochemical staining agent. (Balko & Allison, 2000) A number of TAM$^+$ dye molecules are well known, such as malachite green (MG), brilliant green, crystal violet, and pararosanilin, *etc*. The chemical structures of some of these well-known TAM$^+$ dyes are shown in Fig. 1.

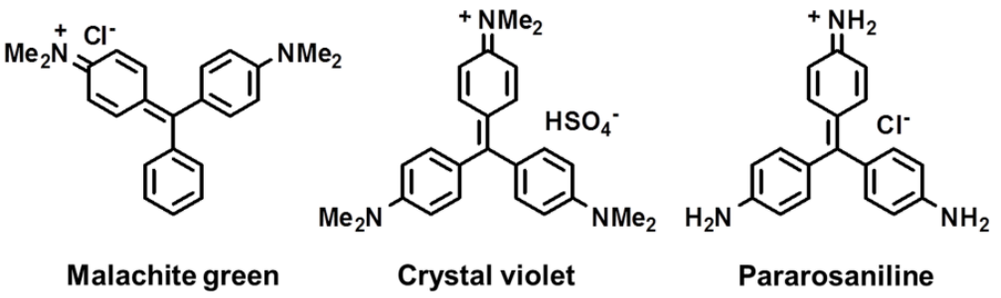

Figure 1. Chemical structures of well-known TAM$^+$ dyes.

Among them, MG is one of the most commonly used chemicals in dye chemistry. MG is a common green dye but it is absorbed into the human body in its carbinol and leuco forms (see the section on UV-Vis spectroscopy). MG is very active with the fungus *Saprolegnia*, which infects fish eggs in commercial aquaculture, and is known to be good for *Ichthyophthirius* in fresh water aquaria. (Indig et al., 2000) It has been known, however, for MG to be highly toxic to mammalian cells, even at low concentrations.(Plakas et al., 1999; Cho et al., 2003) Because of its low cost, effectiveness as an antifungal agent for commercial fish hatcheries, and ready availability, many people can be exposed to this dye through the consumption of treated fish. Since MG is similar in structure to carcinogenic triphenylmethane dyes, it may be a potential human health hazard.

In addition, in their oxidized form, TAM^+ dyes are highly absorbing fluorophores with extinction coefficients of ~2.0×10^5 $mol^{-1}cm^{-1}$ and high quantum yields. Their absorption maxima can easily be matched with the laser lines by simply changing the length of the conjugated chain and/or the heterocyclic moiety. Thus, TAM^+ dyes can be employed as fluorescence labels and sensors of biomolecules *in vivo* because their spectra reach the near-infrared region. Özer (2002) reported efficient non-photochemical bleaching of a TAM^+ dye by chicken ovalbumin and human serum albumin, showing that dye–protein adducts can also form and suggesting that proteins may be primary, rather than indirect, targets of TAM^+ action. However, the use of this substance has been banned in many countries because of its toxicity and possible carcinogenicity. Substitutive materials for MG compounds have thus been in considerable demand. Numbers of researchers (Gessner & Mayer, 2005) have been interested in developing TAM^+ molecules. We developed Fischer's base (FB) analogs of LTAM molecules (Keum et al., 2008, 2009, 2010, 2011, 2012), whose chemical structures contain a couple of heterocyclic FB rings and a substituted phenyl group on a central carbon of the molecules. The structures and numbering system for the Fischer's base (FB) analogs of LTAMs are shown in Fig. 2.

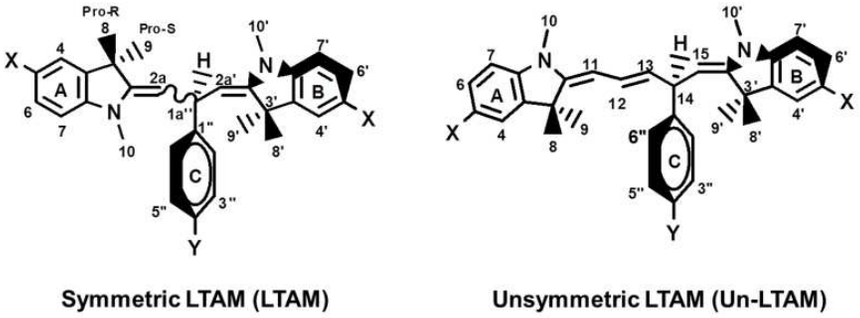

Figure 2. Structures and numbering systems for the FB analogs of symmetric and unsymmetric LTAM molecules.

In this chapter, abbreviations (LTAM and Un-LTAM) will be used to designate the Fischer's base analogs of symmetric and unsymmetric LTAMs, respectively. Note that "the general LTAM" in Section 2.2 denotes the LTAM/TAM^+ dyes that contain no FB moieties.

2. Preparation

2.1. General leuco-TAM and TAM+ molecules

Generally, the Friedel-Crafts-type catalytic alkylation of aromatic rings with aromatic aldehydes is an effective method for TAM+ formation. (Li et al., 2008; Kraus et al., 2008) Several mild and efficient triaryl- and triheteroarylmethanes formations using $[Ir(COD)Cl]_2$-$SnCl_4$, $AuCl_3$, $Cu(OTf)_2$, and $Sc(OTf)_3$ as catalysts have also been reported. Grignard reagents or n-butyl lithium compounds have also been used for their preparation. A brief summary of the preparation methods of general LTAM/TAM+ molecules is shown in Fig. 3.

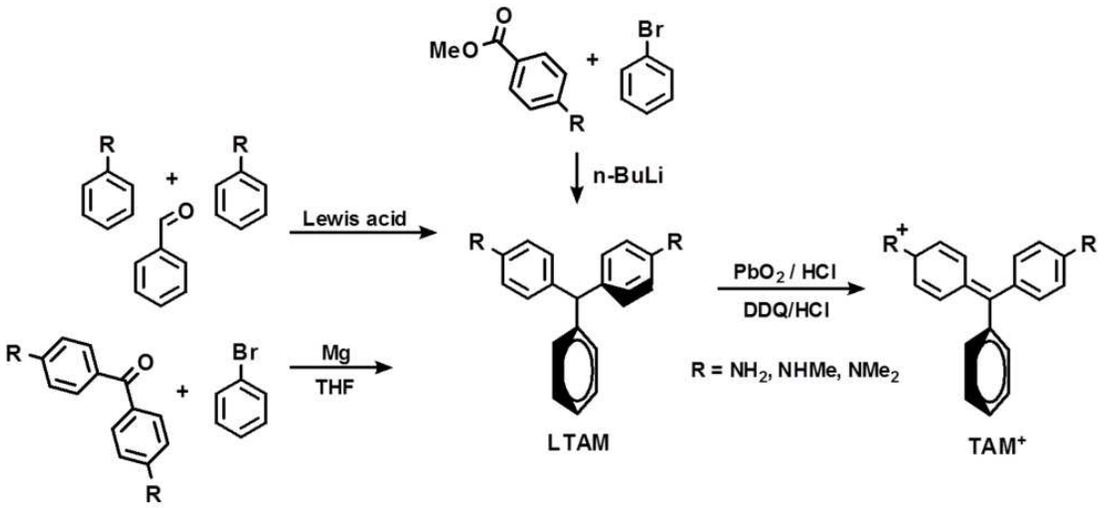

Figure 3. The synthetic procedures for the commercially well-known LTAM molecules.

Although a number of methods are available for the synthesis of triarylmethanes, most are multistep processes and/or require harsh reaction conditions.

2.2. Fischer's base analogs of Leuco-TAM

Fischer's base analogs of LTAM molecules can be obtained from a reaction of a molar excess of Fischer's base and substituted aryl aldehydes. The prepared LTAM dyes consist of two FB rings on the central carbon, where a substituted phenyl ring is located. The LTAM molecules can be symmetric or unsymmetric, depending on the identity of the two FB rings. They are the precursors of the TAM+ dyes, which are structurally close to the polymethine dyes (*e.g.*, Cy3, Cy5, *etc.*). (Ernst et al., 1989)

2.2.1. Symmetric LTAM FB analogs

The FB analogs of symmetric leuco-TAM molecules {2,2′-(2-phenylpropane-1,3-diylidene)bis(1,3,3-trimethylindoline)} derivatives were obtained from the reaction of 5-substituted benzaldehyde and excess (2- to 3-fold) FB in ethanol at room temperature for 2–4 h, as shown in Fig. 4. The white precipitate was filtered from the reaction mixture and washed thoroughly with cold ethyl alcohol. Purification was carried out through

precipitation from acetone. TAM^+ dyes were then obtained from a reaction of LTAM molecule with 2,3-dichloro-5,6-dicyano-1,4-benzoquinone (DDQ) in the presence of HCl, followed by separation of the deep blue form from the product mixtures by column chromatography in MC/MeOH (9:1).

Melting points, yields, and other characteristic data of the prepared LTAM molecules are summarized in Table 1.

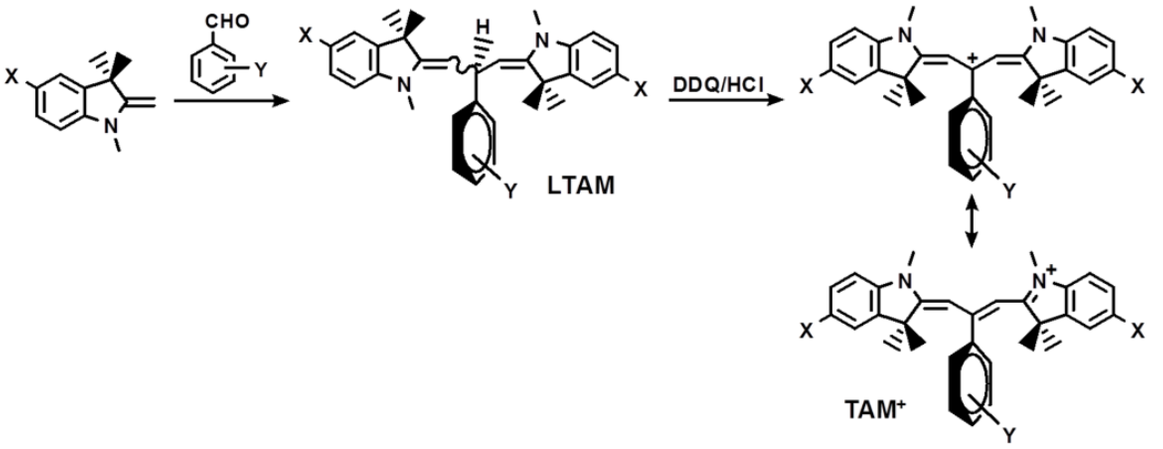

Figure 4. Synthetic scheme for symmetrical LTAM molecules.

2.2.2. Unsymmetric LTAM FB analogs

Unsymmetric LTAMs (Un-LTAM) were obtained from a reaction of excess Fischer's base with the substituted cinnamaldehydes, as shown in Fig. 5. The Un-LTAMs have two different FB skeletons on the central carbon, 1,3,3-trimethyl-2-methyleneindoline and 2-allylidene-1,3,3-trimethylindoline groups. The symmetric TAM^+ dyes with styryl-ring pendants are expected to possess elongated conjugation from the N^+ center of the FB ring to the phenyl ring. However, these LTAM molecules were not successfully obtained from the reactions of Fischer's base with the substituted cinnamaldehydes.

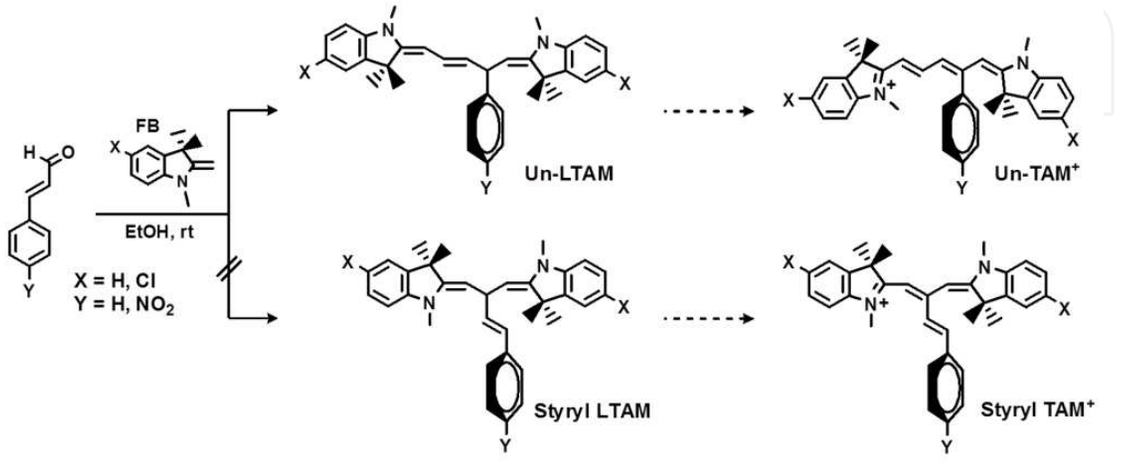

Figure 5. Synthetic scheme for unsymmetrical LTAM molecules.

Experimentally, Un-LTAM molecules were formed as the sole product and no symmetrical LTAM dyes were formed. This suggests that the Michael-type addition of the second molecule of FB occurs on the δ-carbon and not on the β-carbon of the extended α,β-unsaturated iminium salts that were formed from the reaction of FB and cinnamaldehydes. The mechanistic processes for the formation of Un-LTAM molecules are shown in Fig. 6.

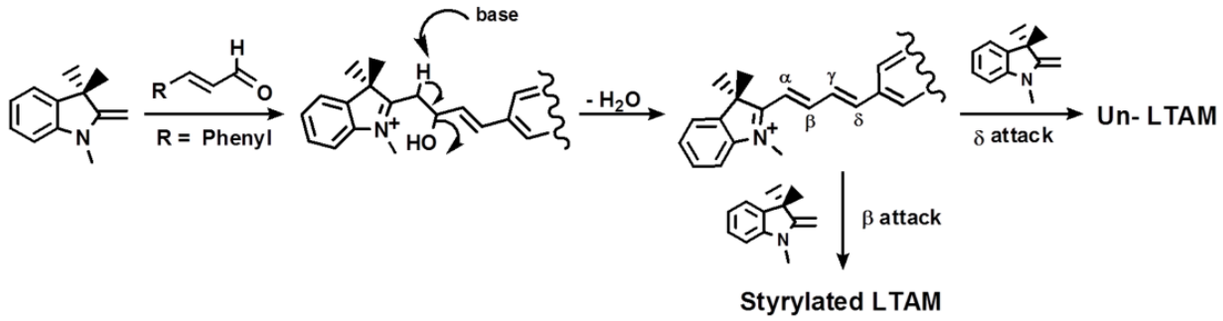

Figure 6. Mechanistic processes of the Michael-type addition of a FB molecule to the β and δ carbon of the α, β, γ, and δ-unsaturated iminium salts to form symmetrical and unsymmetrical LTAM dyes, respectively.

Melting points, yields, and other characteristic data of the prepared LTAM and Un-LTAM molecules are summarized in Table 1.

Compound	LTAM moecule		M.p. (°C)	Yield (%)	Colour
	X	Y			
LTAM **1**	H	H	146	75	white
LTAM **2**	H	*p*-Cl	168	69	pink
LTAM **3**	H	*p*-NO_2	162(dec.)	67	reddish
LTAM **4**	Cl	H	189	82	white
LTAM **5**	Cl	*p*-NO_2	182	89	orange
LTAM **6**	Cl	*m*-NO_2	118(dec.)	72	reddish
LTAM **7**	Cl	2-Cl, 5-NO_2	204	65	orange
LTAM **8**	Cl	*p*-(N)	218-219	89	white
LTAM **9**	Cl	*m*-(N)	189-190	69	white
LTAM **10**	Cl	*p*-OMe	146	57	white
LTAM **11**	Cl	*p*-CHO	157	80	pale orange
LTAM **12**	Benzo[e]	H	181-182	21	pale green
LTAM **13**	Benzo[e]	*m*-(N)	152	48	pale lime
Un-LTAM **1**	H	H	191	42	brown
Un-LTAM **2**	H	*p*-NO_2	186	46	brown
Un-LTAM **3**	Cl	H	182	53	orange
Un-LTAM **4**	Cl	*p*-NO_2	177	55	orange

Table 1. Melting points (M.p.), yields, and colours of the prepared LTAM and Un-LTAM molecules.

3. Spectroscopic Characterization

Newly synthesized FB analogs of LTAM molecules are not expected to be fully planar because of steric crowding, rather they can be viewed as a screw or helical, and thus may possess propeller structures. Subsequently, they can adopt a conformation where all three rings are twisted in the same direction, making a right- or left-handed propeller. As an analogy to a common screw or bolt, right- and left-handed screws are nominated as *M* and *P*, respectively, as shown in the upper line of Fig. 7. The red arrows denote the direction of bond rotation, not the helical direction (blue arrows). Two rings rotate through a perpendicular conformation while one moves in the opposite direction.

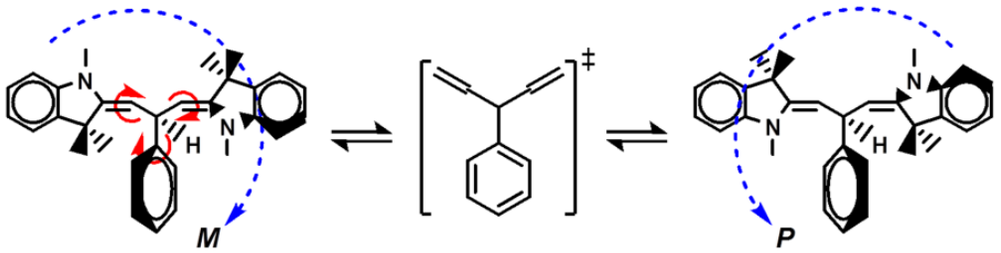

Figure 7. A new diastereomer can be formed via bond rotation (red arrows) of one diastereomer (blue arrows denote the helical direction between *M* and *P* isomers).

Theoretically, three configurational isomers, *ZE*, *EE*, and *ZZ*, can be proposed for these dyes. Since the *ZE* isomers can have *M* and *P* conformations, *ZE*-LTAM molecules can be obtained as a racemic mixture from the synthetic reaction described previously.

3.1. Diastereomeric identification for the prepared LTAM molecules by 1D ^{1}H NMR and 2D NMR experiments

The ^{1}H NMR spectra of LTAM molecules display characteristic signals (three groups) in the aliphatic region, namely a triplet and two doublets (group A) in the range of 4.20–5.40 ppm, two singlets (group B) between ~2.90 and ~3.30 ppm, and four identical singlets (group C) at 1.20–1.80 ppm. As a representative example, the ^{1}H NMR spectrum of LTAM **4** in $CDCl_3$ is shown in Fig. 8.

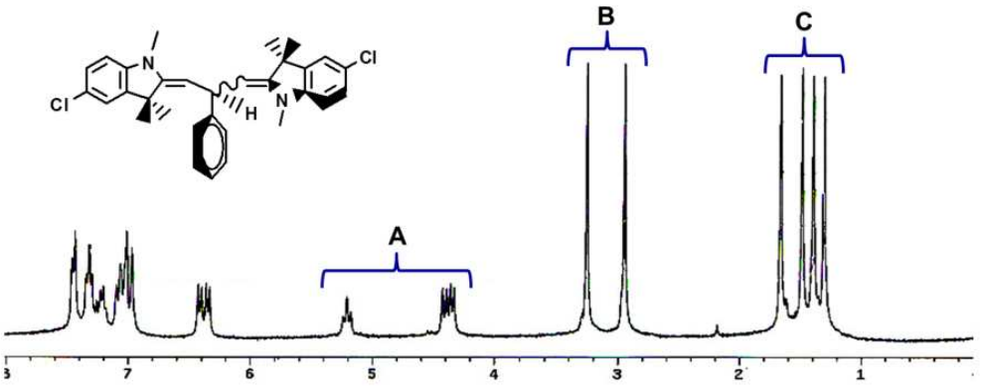

Figure 8. ^{1}H NMR spectroscopy of LTAM **4** as a representative example.

Judging from the chemical shifts of the signals in Fig. 8, group A may belong to sp^2 protons, H2a and H2a' and allylic proton H1a'', and groups B and C may belong to *N*-Me (H10) and *gem*-dimethyl groups (H8 and H9), respectively. Interestingly, the *gem*-dimethyl groups show four well-separated singlets, indicating that these *gem*-dimethyl groups are diastereotopic. Thus, the *gem*-dimethyl groups are not identical and they have different chemical shifts in the NMR spectra. The most common instance of diastereotopic groups is when two similar groups are substituents on a carbon adjacent to a stereogenic center. These LTAM molecules may not be fully planar because of steric crowding and would thus be expected to exhibit chirality, having no stereogenic centers. No detailed discussions are not given for the resoncances in the range of 6 to 8 ppm, since the resonance in those ranges are of the general aromatic protons.

The ^{1}H and ^{13}C resonances of the LTAM molecules were assigned using COSY and one-bond ^{1}H–^{13}C correlations obtained by both direct-detection HETCOR and indirect detection HSQC experiments. COSY was used to identify peaks from the A and B rings. The HETCOR and HSQC identified the shifts of the proton-containing carbons. HMBC was used to differentiate between the two A and B rings of one half of the molecules because these rings were not identical.

The HETCOR experiment identified the carbon shifts of those carbons with protons attached through one-bond coupling between ^{1}H and ^{13}C. Correlations between the protons such as H2a, H8, H9, H10 and H1a'', and their corresponding carbons are particularly useful for structure determination, as indicated in Fig. 9.

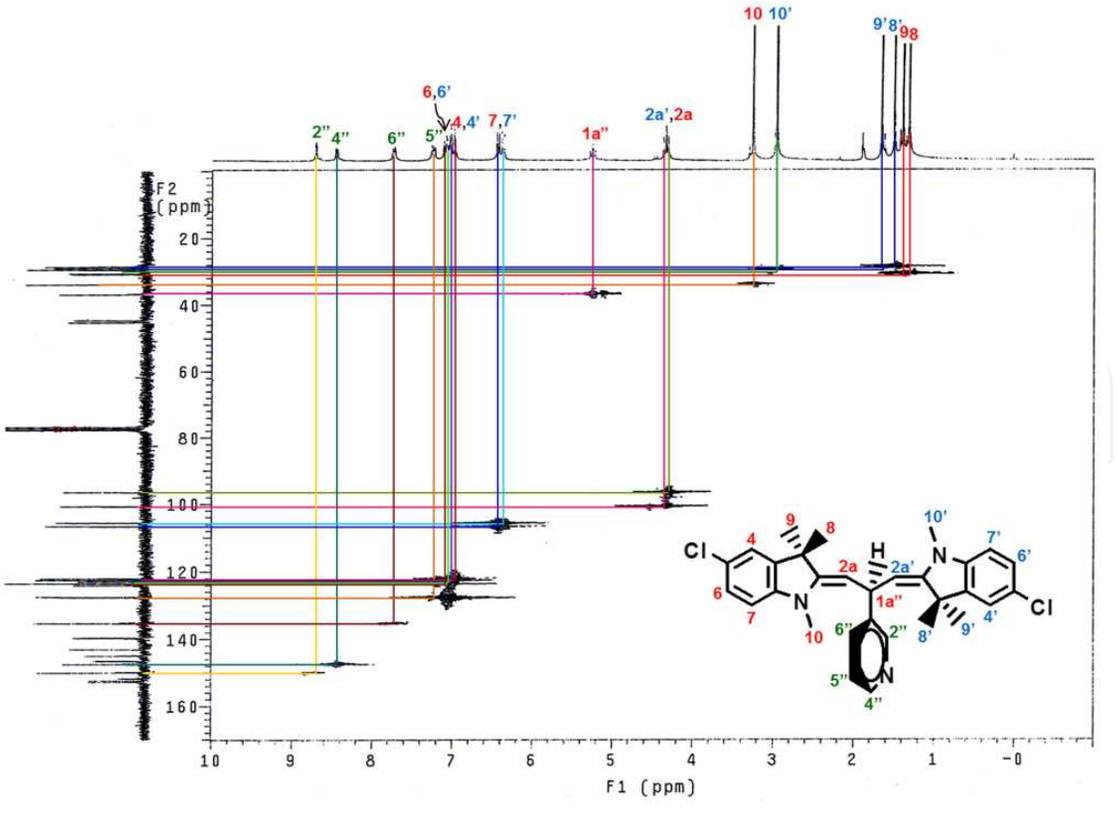

Figure 9. HETCOR of LTAM **9** in the range of of 0-170 ppm.

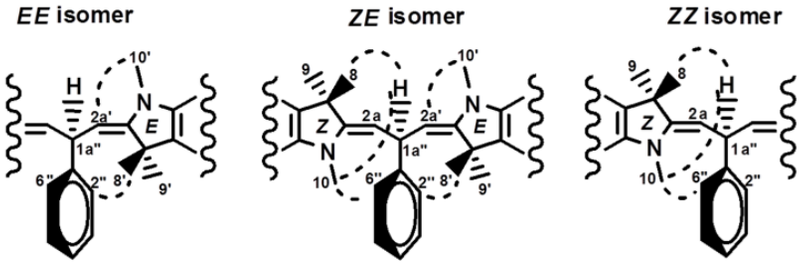

Figure 10. Structures and NOE correlations of the *ZE*, *EE*, and *ZZ* isomers of LTAM molecules.

The major chemical shift assignments within FB rings, A and B, of the molecules were mostly made using HMBC and NOE data. Since A and B rings are not identical, HMBC was needed to differentiate between the two groups of FB molecules. HMBC experiments have thus correlated C2 to H1a'', H2a, H8, H9, and H10 of ring A and correlated C2' to H1a'', H2a', H8', H9', and H10' in ring B. For the geometrical identification around the double bonds of the enamine moiety of the A and B (FB) rings, NOE experiments were carried out. Structures and NOE correlations of the *ZE*, *EE*, and *ZZ* isomers of the LTAM molecules are shown in Fig. 10. Determination of the configuration of the double bonds at positions 2–2a and 2'–2a' of the enamine moiety of the A and B (FB) rings was carried out by an NOE experiment. Strong NOE correlation was observed between the protons H10' (*N*-Me of B) at 2.97 ppm and H2a' (the same subunit) at 4.42 ppm. In addition, H10 (*N*-Me of A) has NOE with H2''/H6'', whereas the *gem*-dimethyl, H8 and H9, exhibits NOE with H2a. These observations are compatible with a *Z* arrangement around the double bond of ring A.

Compound	H or C	*Z* Ring		*E* Ring		Others[a]	
		δ (H)	δ (C)	δ (H)	δ (C)	δ (H)	δ (C)
	2/2'	-	151.6	-	151.3	-	-
	2a/2a'	4.36(d)	97.3	4.42(d)	101.5	-	-
	3/3'	-	44.8	-	44.2	-	-
	3a/3a'	-	139.4	-	139.6	-	-
LTAM **4**	8/8'	1.32(s)	30.6	1.50(s)	28.6	-	-
	9/9'	1.41(s)	30.8	1.68(s)	29.0	-	-
	10/10'	3.26(s)	33.5	2.95(s)	29.2	-	-
	1a''	-	-	-	-	5.22(dd)	38.7
	2''/6''	-	-	-	-	7.46(d)	127.6
	2/2'	-	-	-	155.8		
	2a/2a'	-	-	4.42	100.5		
	3/3'	-	-	-	45.16		
	3a/3a'	-	-	-	139.6		
LTAM **5**[b]	8/8'	-	-	1.39	30.6		
	9/9'	-	-	1.60	28.6		
	10/10'	-	-	2.97	29.0		
	1a''	-	-	-	-	5.19(t)	38.8
	2''/6''	-	-	-	-	7.53(d)	128.8

Compound	H or C	*Z* Ring		*E* Ring		Others[a]	
		δ (H)	δ (C)	δ (H)	δ (C)	δ (H)	δ (C)
LTAM **8**[b]	2/2'	-	-	-	152.0	-	-
	2a/2a'	-	-	4.41(d)	100.1	-	-
	3/3'	-	-	-	44.7	-	-
	3a/3a'	-	-	-	139.6	-	-
	8/8'	-	-	1.41(s)	29.3	-	-
	9/9'	-	-	1.51(s)	28.4	-	-
	10/10'	-	-	2.97(s)	28.6	-	-
	1a''	-	-	-	-	5.07(t)	38.3
	2''/6''	-	-	-	-	7.31(d)	122.9
LTAM **10**	2/2'	-	151.6	-	151.2	-	-
	2a/2a'	4.30(d)	97.9	4.37(d)	102.3	-	-
	3/3'	-	44.9	-	44.3	-	-
	3a/3a'	-	139.6	-	139.9	-	-
	8/8'	1.30(s)	30.8	1.47(s)	29.4	-	-
	9/9'	1.39(s)	30.7	1.65(s)	28.6	-	-
	10/10'	3.25(s)	33.7	2.94(s)	28.9	-	-
	1a''	-	-	-	-	5.15(dd)	37.8
	2''/6''	-	-	-	-	7.35(d)	127.4

[a]Others denote the phenyl ring and connecting groups of the LTAM molecules.

[b]Compound that has the *EE* configuration as the major isomer.

Table 2. ^{1}H and ^{13}C NMR spectral data for LTAM molecules in $CDCl_3$ (500 and 125 MHz, respectively).

Similarly, H2a' and H9' have NOE correlations with H10' and H2''/H6'', respectively. These NOE phenomena indicate a *ZE* geometry around the double bonds of the enamine moieties of A and B (FB) rings, respectively. Selected ^{1}H and ^{13}C NMR spectral data for the major diastereomer of various LTAM molecules in $CDCl_3$ (500 and 125 MHz, respectively) are listed in Table 2.

3.2. Thermal diastereomerization

3.2.1. Diastereomeric mixtures in equilibrium state

The ^{1}H NMR spectra of LTAM **4** became complicated upon thermal treatment. After approximately 2 h they exhibited three sets of signals corresponding to two other forms (a & b) in addition to the original major set, in $CDCl_3$, as shown in Fig. 11. Two of the double bonds in the LTAM molecules can exist as *ZE*, *EE*, and *ZZ* isomers, which may account for the complexity of the spectra. Their existence is most likely due to geometrical isomerism with respect to restricted rotation around the C=C double bond of the FB moiety and the C-CH(FB)(Ph) single bonds.

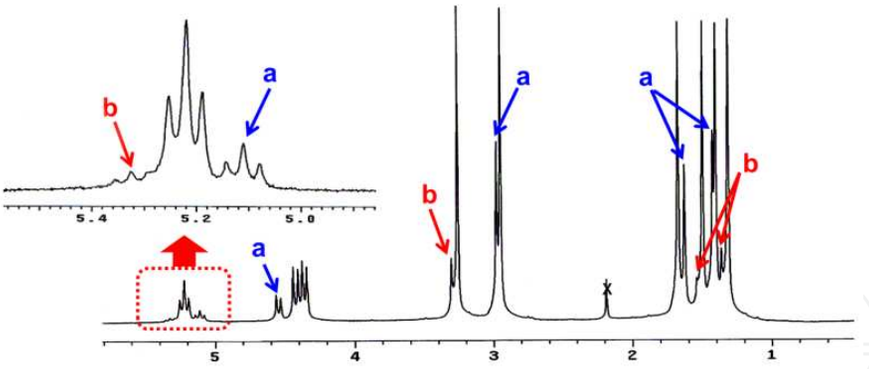

Figure 11. ^{1}H NMR spectra of LTAM **4** at the thermal equilibrium state, showing three sets of analog peaks (major, a and b groups).

Detailed analysis of the ^{1}H NMR spectra of the LTAM compounds in the thermal equilibrium state is important for determining the presence of a mixture of *ZE* and *EE* or *ZZ* isomers. After thermal equilibrium of LTAM **4** in $CDCl_3$, 2 h after sampling in an NMR tube at room temperature, three sets of complex signals were observed, namely triplet peaks at 5.0–5.4 ppm, three doublets at 4.3–4.6 ppm, four singlets at 2.8–3.4 ppm, and eight singlets at 1.3–1.7 ppm. Among these peaks, those signals assigned to the *ZE* isomers were a triplet at 5.22 ppm, two doublets at 4.36 and 4.42 ppm, two singlets at 2.95 and 3.26 ppm, and four singlets at 1.3–1.7 ppm, as discussed previously. The residual peaks might belong to the *EE* and/or *ZZ* isomers.

For identification of each of the diastereomers of LTAM **4** in organic solvents, 2D NMR experiments such as COSY, HMBC, and NOESY, were used at the equilibrium state. As an example, a COSY of diastereomeric mixtures of LTAM **4** in the range of 4.25–5.25 ppm in $CDCl_3$ is given in Fig. 12.

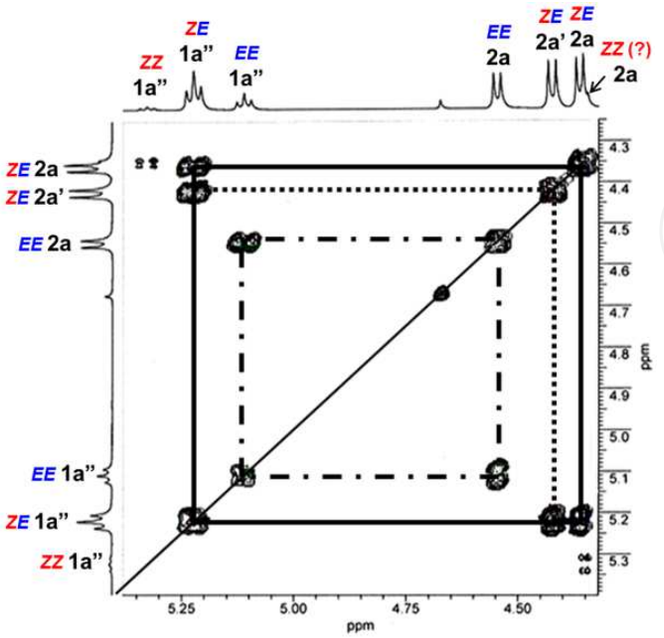

Figure 12. COSY of diastereomeric mixtures of LTAM **4** in the range of 4.25–5.25 ppm in $CDCl_3$.

^{1}H-^{1}H COSY in the range of 4.25–5.25 ppm showed two individual sets of H1a'' and H2a/2a' protons for the diastereomeric structures *ZE* (solid and dot) and *EE* (dash-dot) isomers of LTAM **4**, respectively. The methylene doublets of the *ZZ* isomers for this compound could not be detected due to their low concentration in the equilibrium state. Three sets of *N*-Me (H10 or H10') in the range of 2.8–3.4 ppm and the germinal methyl group (H8 and H9, and H8' and H9') could be easily distinguished through the visual peak ratios of the ^{1}H NMR.

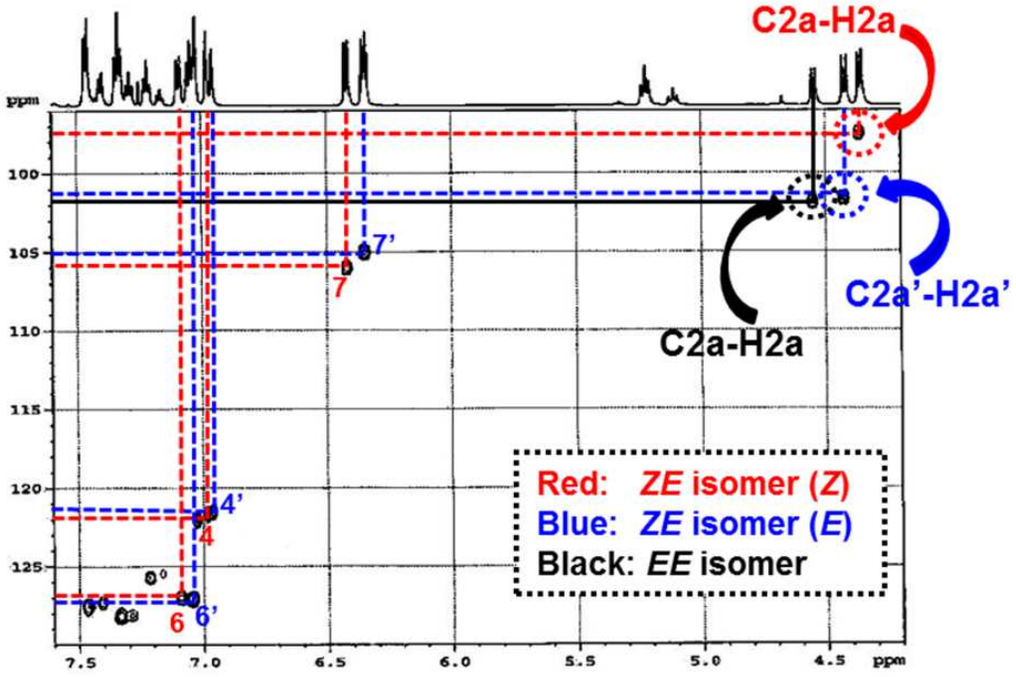

Figure 13. HSQC of diastereomeric mixtures of LTAM **4**, showing one-bond correlation of C2a-H2a, C2a'-H2a' for the *ZE* isomer and C2a-H2a for the *EE* isomer in the range of 95-130ppm.

^{1}H–^{13}C correlations were obtained by both direct-detection HETCOR and indirect detection HSQC experiments. Fig. 13 shows some of the one-bond ^{1}H–^{13}C correlations. HSQC identifies the shifts of the carbons bearing protons of the major *ZE* and minor *EE* isomers.

More particularly, HMBC can identify which protons belong to which unit. For the major *ZE* isomers, HMBC experiments have correlated C2 to H1a'', H2a, H8, H9, and H10 of ring A and correlated C2' to H1a'', H2a', H8', H9', and H10' in ring B. The *gem*-dimethyls (1.50 and 1.68 ppm) are correlated with C3' at 44.2 ppm. The H2a' at 4.42 ppm is correlated to the same C3', which allow us to assign it to the same subunit (B ring). Similarly, the *N*-Me at 2.95 ppm, correlated to the same C3', is also in the same subunit (B ring). The other *gem*-dimethyl groups (1.32 and 1.41 ppm) are correlated with C3 at 44.8 ppm. The H2a at 4.36 ppm and the *N*-Me at 3.26 ppm are also correlated to the same C3, indicating that they are in the second subunit (A ring). The low-field HMBC of the diastereomeric mixtures of LTAM **4** is given in Fig. 14 and the high-field HMBC (< 95 ppm) are not given here.

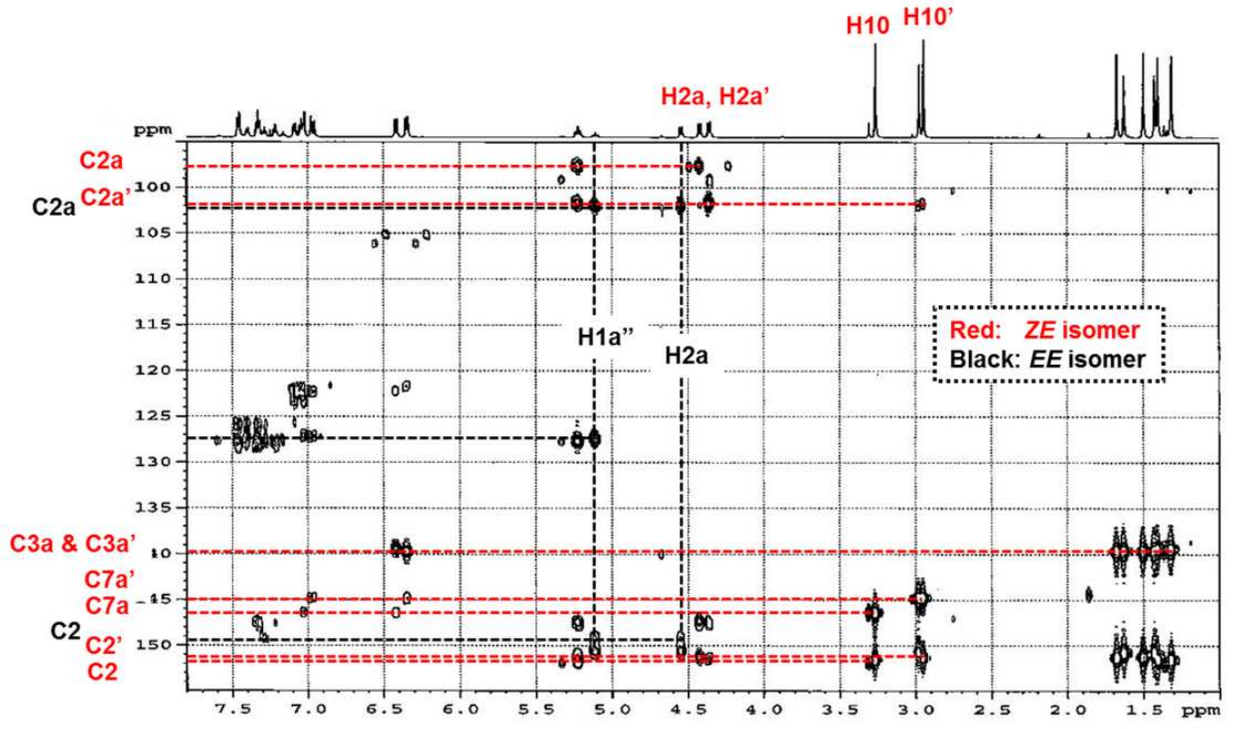

Figure 14. HMBC of the diastereomeric mixtures of LTAM **4** in the range of 95–155 ppm.

For the minor concentration *EE* isomers, the HMBC experiments correlated C2 at 149 ppm to H1a'', H2a, H8, H9, and H10. Similar correlations of C3 were made for H2a, H4, H8, and H9. HMBC could further correlate C3a to H7, H8, and H9. Similar to the extremely minor *ZZ* isomers, HMBC correlated C2 to H1a'', H2a, H8, H9, and H10.

Similar correlations of C3 were made to H2a, H4, H8, and H9. HMBC further correlated C3a to H7, H8, and H9. These correlations provided a clear distinction between diastereomeric isomers. H2a and *N*-Me were also coupled to the same C3, which confirms that all of the protons belong to the same isomer. As H9 or *N*-Me is coupled to C2''/C6'', the protons of the aromatic ring could be identified as a substructure of each isomer.

2D NOESY showed spatial correlations for each of the diastereomeric mixtures for LTAM **4** after reaching thermal equilibrium, as in Fig. 15. Namely, the spatial correlations labeled a–f in red were detected for the *ZE* isomer, and those labeled b', d', and f' in blue are detected for the *EE* isomer. In addition, one correlation, e' in green, was detected for the *ZZ* isomer.

Unfortunately, a few of the ^{1}H resonance peaks for the *ZZ* isomers were able to be detected, such as an *N*-methyl singlet and, very rarely, two *gem*-dimethyl peaks. This result indicates that the LTAM molecules equilibrate in a time-dependent manner, yielding a mixture of the *ZE*/*EE*/*ZZ* isomers in organic solvent ($CDCl_3$).

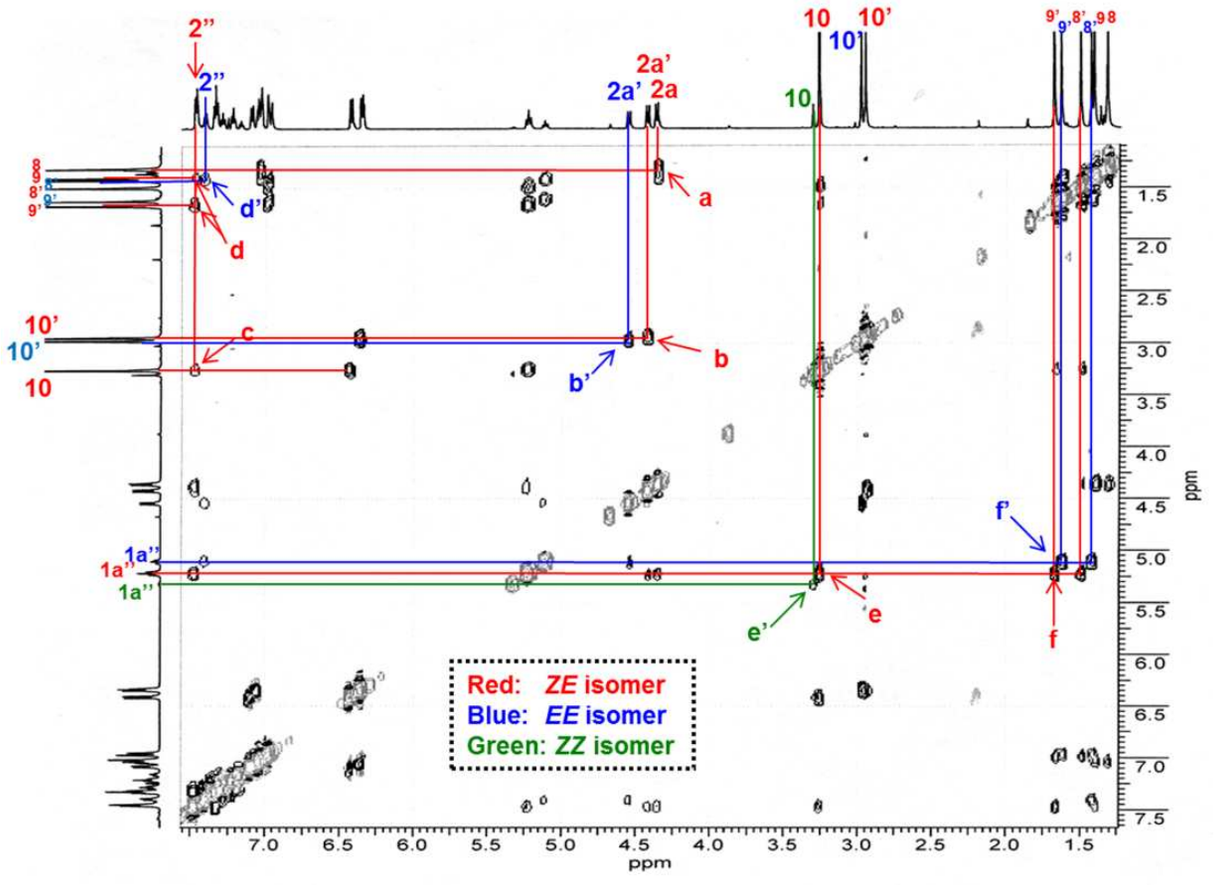

Figure 15. 2D NOESY of the diastereomeric mixtures of LTAM **4** after reaching thermal equilibrium in $CDCl_3$.

This NOE phenomenon indicates a *ZE* geometry around the double bonds of the enamine moieties of A and B (FB) rings of the major isomer. However, the minor isomer contains two symmetric Fischer's base units and 2D NOESY only showed the correlations of H2a'-H10' (blue mark, b'), H8'-H2''/H6'' (blue mark, d') but no correlation of H10'-H2''/H6''. This suggests that the *ZE* geometry around the double bonds of the enamine moieties does not exist for the minor isomer. Although the spatial correlations of H2a-H9, H10-H2''/H6'' and H1a''-H10 were expected for the extremely minor *ZZ* isomer, the proton peaks H2a and H2a' of the *ZZ* isomer were too small to be correlated with other protons in the 2D NOESY experiment. One spatial correlation of H1a''-H10 (green mark, e') was detected. This NOE phenomenon indicates that three diastereomers, such as *ZE*, *EE*, and *ZZ*, are in equilibrium with various ratios among the diastereomeric isomers, depending on the NMR solvent used.

The NMR data for the *Z* or *E* ring of the *ZE* isomer suggest that the signals for the geminal dimethyl group for the *EE* isomer should be shifted downfield compared to those of the *ZZ* isomer, whereas the signals of the *N*-methyl groups should be shifted upfield. The geminal dimethyl group signals for the *EE* isomer were shifted upfield compared to those of the *ZE* isomer, whereas the signals of the *N*-methyl and methylene groups were shifted downfield.

Compound	Ring	proton	Diastereomer (ppm)		
			ZE	*EE*	*ZZ*
LTAM **1**	*Z*	8-Me	1.31	-	1.37
		9-Me	1.41	-	1.57
		N-Me	3.28	-	3.32
		H2a	4.33	-	N/A
	E	8'-Me	1.51	1.44	-
		9'-Me	1.68	1.64	-
		N'-Me	2.97	3.00	-
		H2a'	4.41	4.53	-
LTAM **2**	*Z*	8-Me	1.33	-	1.38
		9-Me	1.42	-	1.55
		N-Me	3.29	-	3.33
		H2a	4.31	-	N/A
	E	8'-Me	1.52	1.46	-
		9'-Me	1.68	1.64	-
		N'-Me	2.99	3.01	-
		H2a'	4.36	4.47	-
LTAM **4**	*Z*	8-Me	1.32	-	N/A
		9-Me	1.41	-	N/A
		N-Me	3.26	-	N/A
		H2a	4.36	-	N/A
	E	8'-Me	1.50	1.43	-
		9'-Me	1.68	1.63	-
		N'-Me	2.95	2.98	-
		H2a'	4.42	4.55	-
LTAM **5**	*Z*	8-Me	1.30	-	N/A
		9-Me	1.39	-	N/A
		N-Me	3.22	-	3.28
		H2a	4.31	-	N/A
	E	8'-Me	1.41	1.39	-
		9'-Me	1.65	1.60	-
		N'-Me	2.94	2.97	-
		H2a'	4.32	4.42	-
LTAM **10**	*Z*	8-Me	1.30	-	N/A
		9-Me	1.39	-	N/A
		N-Me	3.25	-	3.28
		H2a	4.30	-	N/A
	E	8'-Me	1.47	1.41	-
		9'-Me	1.65	1.60	-
		N'-Me	2.94	2.96	-
		H2a'	4.37	4.49	-
LTAM **12**	*Z*	8-Me	1.67	-	N/A
		9-Me	1.77	-	N/A
		N-Me	3.44	-	N/A
		H2a	4.47	-	N/A
	E	8'-Me	1.90	1.83	-
		9'-Me	2.06	2.04	-
		N'-Me	3.08	3.11	-
		H2a'	4.52	4.60	-

Table 3. Selected ^{1}H resonances for some of the diastereomeric LTAMs.

Deshielding of the *gem*-dimethyl proton of the *EE* and the *N*-methyl proton of the *ZZ* isomer may be due to their relative proximity to the benzene ring, as indicated in the *ZE* isomers. Selected ^{1}H resonances for the diastereomeric LTAMs are listed in Table 3.

3.2.2. Dynamic behavior of LTAM molecules

Interestingly, the stability of these molecules in solution depends upon the solvent media. Namely, they are inert in polar organic solvents such as acetone and DMSO, but they are unstable in nonpolar solvents such as benzene, THF, and chloroform. They equilibrate time-dependently into a mixture of *ZE*/*EE* or *ZE*/*EE*/*ZZ* isomers, depending on the solvents used, as shown in Fig. 16.

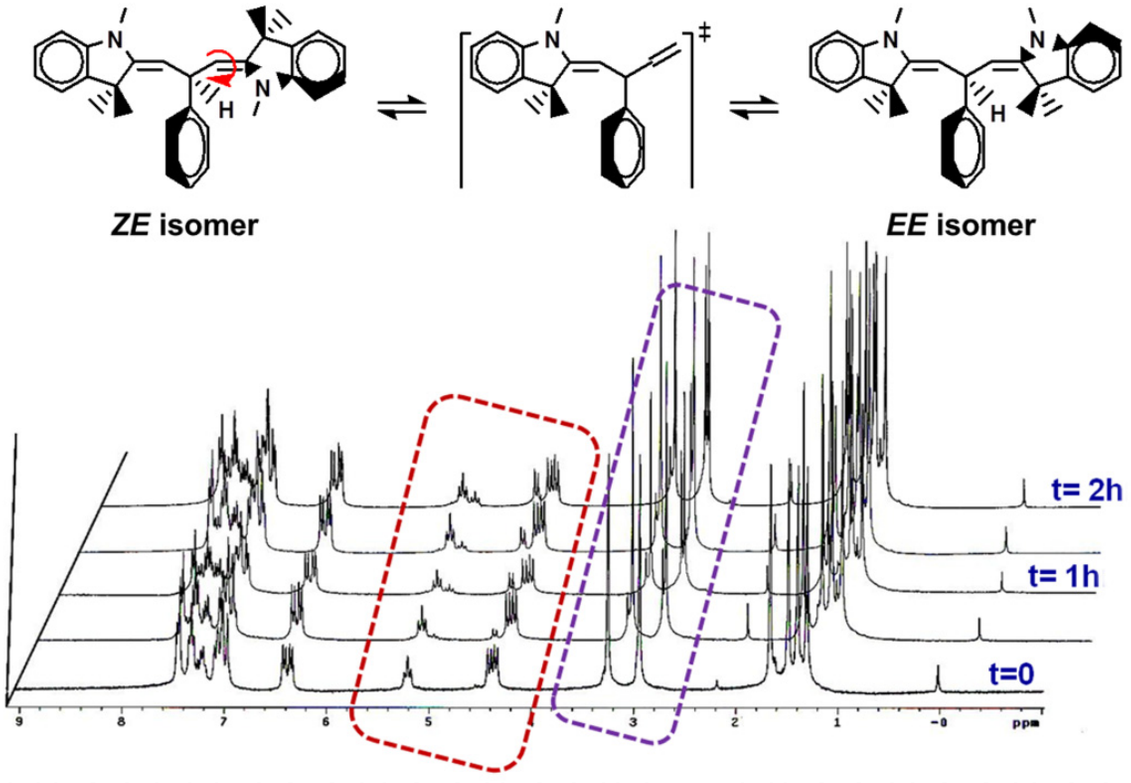

Figure 16. Dynamic behavior of LTAM **1** in $CDCl_3$, showing diastereomeric isomerization.

It has been reported (Keum et.al. 2008) that FB-analogs of LTAM molecules have very characteristic ^{1}H NMR resonance patterns in the range of 1.0–5.4 ppm as a result of three consecutive protons (H2a, H2a', and H1a''), two *N*-methyl, and four diastereotopic *gem*-dimethyl (8- and 9-Me) groups. Therefore, these characteristic peaks can be used to discriminate each of the diastereomers. (Ma et al., 2012) For example, ^{1}H NMR data of the 3-pyridinyl LTAM **9** showed the expected features (A → B) of resonances, *viz*. one triplet at 5.25 ppm, two doublets at 4.31 and 4.34 ppm, two singlets at 2.95 and 3.25 ppm, and four singlets at 1.30–1.65 ppm. In contrast, the spectra of 4-pyridinyl LTAM **8** showed very interesting features in the range of 2.90–5.40 ppm. This compound showed one triplet at 5.07 ppm, a doublet at 4.41 ppm, and a singlet at 2.97 ppm, as shown in C of Fig. 17.

The isomerization pattern of LTAM **8** is quite surprising because no FB-analog of MG showed a LTAM **8**-like feature (C → B) in the range of 2.90–5.40 ppm. Based upon quantum mechanical calculations (Keum et al., 2010), *ZE* would be expected to predominate over *ZZ* and *EE* in all media. Experimentally, the *ZE* isomers of LTAM compounds generally predominant in all organic media examined. The relative energy differences between the minor *EE* and extremely minor *ZZ* were 0.08 and 0.26 kcal/mol in $CDCl_3$ and DMSO-d_6, respectively. In addition, both of the spectra, A and C, converged to that displayed by B approximately 2–3 h after mixing the LTAM molecules with $CDCl_3$ in the NMR tube.

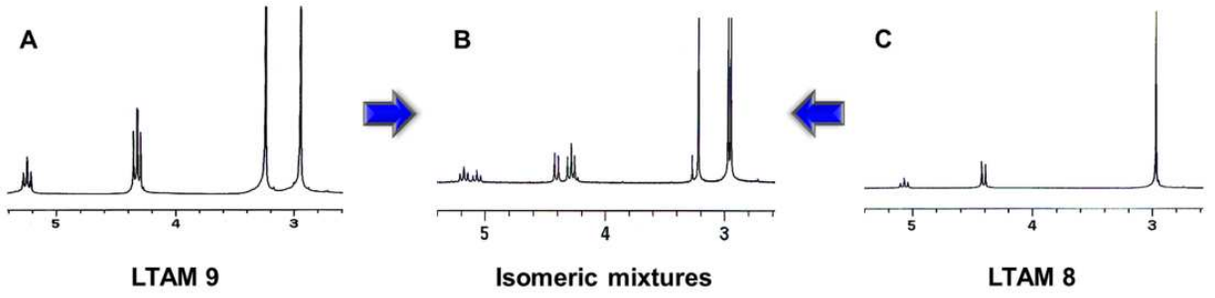

Figure 17. Characteristic proton resonance of the LTAM molecules in the range of 2.80~5.40 ppm in $CDCl_3$ (A: *ZE*, B: mixture after reaching thermal equilibrium, and C: *EE* diastereomer); arrows show the directions of isomerization.

3.2.3. Determination of diastereomeric ratios at equilibrium state

Since the characteristic peaks can be used to discriminate each of the diastereomers, the equilibrium ratios among these diastereomeric isomers in various organic solvents can be determined by ^{1}H NMR spectra. This is based on the intensities of either the *N*-methyl or *gem*-dimethyl signals corresponding to the three diastereomeric isomers at the equilibrium state. In some cases, the intensity of the H1a'' proton of the central carbon can be used. Since the *N*-methyl peaks show a well-separated singlet, it is more convenient to measure the ratio of the isomers. The cause of the isomerization of the LTAM compounds at room temperature is unclear. They belong to the group of conjugated enamine compounds. Enamine-imine tautomerism (C=C-NH and CH-C=N) may regulate *ZE* isomerization.

For most of the LTAM molecules examined that are listed in Table 1, the *ZE* isomers are the most stable and they at the equilibrium state for almost 100% of the time in polar solvents ($E_T(30) > 42$) and 60–80% in non-polar solvents ($E_T(30) < 42$) at room temperature. The minor *EE* minor and extremely minor *ZZ* isomers at the equilibrium state were 18–44% and 0–11% in nonpolar solvents, respectively, depending on the molecules examined. The percent ratios among the diastereomeric isomers of LTAM molecules in the thermal equilibrium states vary according to the molecules examined and solvents used.

However, some LTAM molecules, such as LTAMs **3**, **5**, and **8**, are exceptional. Surprisingly, the pure *EE* isomers are obtained, unlike for the LTAM molecules described previously. These exceptional compounds contain a resonance-electron withdrawing (-R) substituent, particularly on the para-position of the phenyl ring. This indicates that substituents such as

p-NO_2, *p*-CHO, or *p*-(N) on the phenyl ring make the *EE* isomer more stable than the *ZE* isomer, which is predicted to be more stable theoretically. These are summarized in Table 4.

Further detailed studies are needed to determine how the isomerization occurs and what causes the unusual stability of a certain diastereomer.

Compound	Solvent	Percent ratio (%)			K_{eq}[a]	Note[b]
		ZE	*EE*	*ZZ*		
LTAM **4**	$CDCl_3$	60.2	28.3	11.4	1.52	*ZE*
	Aceton-d_6	68.5	25.9	5.60	2.17	
	DMSO- d_6	91.5	8.5	-	10.76	
LTAM **5**	$CDCl_3$	61.0	34.1	4.90	0.52	*EE*
	Aceton-d_6	59.9	34.8	5.30	0.53	
	DMSO- d_6	33.2	68.8	-	2.07	
LTAM **8**	$CDCl_3$	63.3	31.3	5.40	0.46	*EE*
	Aceton-d_6	61.3	32.8	5.90	0.49	
	DMSO- d_6	36.4	63.6	-	1.75	
LTAM **9**	$CDCl_3$	64.0	31.1	4.80	1.78	*ZE*
	Aceton-d_6	62.4	32.0	5.60	1.66	
	DMSO- d_6	59.2	40.8	-	1.45	
LTAM **10**	$CDCl_3$	67.1	27.4	5.50	2.03	*ZE*
	Aceton-d_6	65.8	27.7	6.50	1.92	
	DMSO- d_6	80.7	13.0	6.30	4.18	

[a]K_{eq} is the ratio of [*ZE*]/[*EE*+*ZZ*] or [*EE*]/[*ZE*+*ZZ*], depending on the identity of the major diastereomer.

[b]The major isomer in the solid state.

Table 4. Percent ratios among the diastereomeric isomers of LTAM molecules at thermal equilibrium states.

3.2.4. Free energy change of activation, ΔG‡

The rate constants for the formation of the *EE* (and *ZZ)* isomers were measured from a plot of ln(A−A_∞) versus time (in min), according to the peak-intensity of the central proton at ~5.15 ppm. As an example, excellent linearity was obtained with r = 0.999 and n = 6. The k_{obs} and half-life ($t_{1/2}$) for the isomerization of LTAM **4** were 5.95×10^{-4} s^{-1} and 19.4 min, respectively. The first-order rate constant is a sum of the rate constants for the backward and reverse reactions. From the rate constant obtained at room temperature, the obtained one-temperature $\Delta G^{\ddagger}$ value (Dougherty et al., 2006) for the *ZE* → *EE* isomerization of LTAM **4** in $CDCl_3$ was found to be 21.8 kcal/mol. Similarly, the rate constants for the diastereomeric isomerization of LTAM molecules were measured and the one-temperature $\Delta G^{\ddagger}$ values of all of them were obtained, using the equation 1 (Dougherty et.al. 2006) given below:

$$\Delta G^{\ddagger} = 4.576\ [10.319 + \log (T/k)]\ \text{kcal/mol} \quad (1)$$

These are summarized in Table 5.

Compound	k_{obs} x10^{-4} s^{-1}	$t_{1/2}$ (min)	Linearity		$\Delta G^{\ddagger}_{ZE \rightarrow EE}$	$\Delta G^{\ddagger}_{EE \rightarrow ZE}$
			r	n		
LTAM **4**	5.95	19.4	0.999	6	21.8	-
LTAM **5**	0.43	297	0.999	3	-	23.4
LTAM **8**	2.72	42.5	0.999	6	-	22.3
LTAM **9**	4.66	24.8	0.994	4	22.0	-
LTAM **10**	2.48	46.5	0.998	5	22.0	-
LTAM **11**	4.72	24.5	0.998	5	-	22.4
LTAM **13**	17.9	6.47	0.998	3	21.2	-

Table 5. Rate constants and $\Delta G^{\ddagger}$ values for the *ZE*/*EE* isomerization of LTAM molecules in $CDCl_3$.

It has been previously reported that the *ZE* isomerization of imines and their tautomeric isomers, enamines, has a very high energy barrier ($\Delta G^{\ddagger}$ = 23 kcal/mol), unless the process is strongly accelerated by either acid/base catalysts or by push-pull substituents. (Liao & Collum, 2003). The isomerization rate was found to be slow on the NMR time-scale.

3.3. UV-Vis spectroscopy of various forms of LTAM molecules

FB analogs of TAM^+ dyes were obtained from the reaction of FB analogs of LTAM molecules with DDQ in the presence of HCl, followed by separation of the deep blue form from the product mixtures by column chromatography in MC/MeOH (7:1). A reaction of TAM^+ with an inorganic base such as NaOH gives the carbinol form of the LTAM molecule. Only the TAM^+ cation shows deep coloration, in contrast to the LTAM and carbinol derivatives. This difference arises because only the cationic form has extended π-delocalization, which allows the molecule to absorb visible light.

The colored forms, TAM^+, of the prepared LTAM and Un-LTAM molecules have absorption maxima at 580–705 and 350–420 nm in ethanol for the x- and y-band, respectively. The carbinol form was detected at 325–385 nm in basic media. The leuco form of these molecules decomposed in HCl-saturated EtOH to form conjugated molecules observed at 385–435 nm. UV-Vis spectral data in $CDCl_3$ of the colored and decomposed forms LTAM **4**, and Un-LTAM **4**, as representative examples, are shown in Fig. 18.

UV-Vis spectral data for various forms of LTAM and Un-LTAM molecules, compared to those of commercial TAM^+ dyes, are summarized in Table 6.

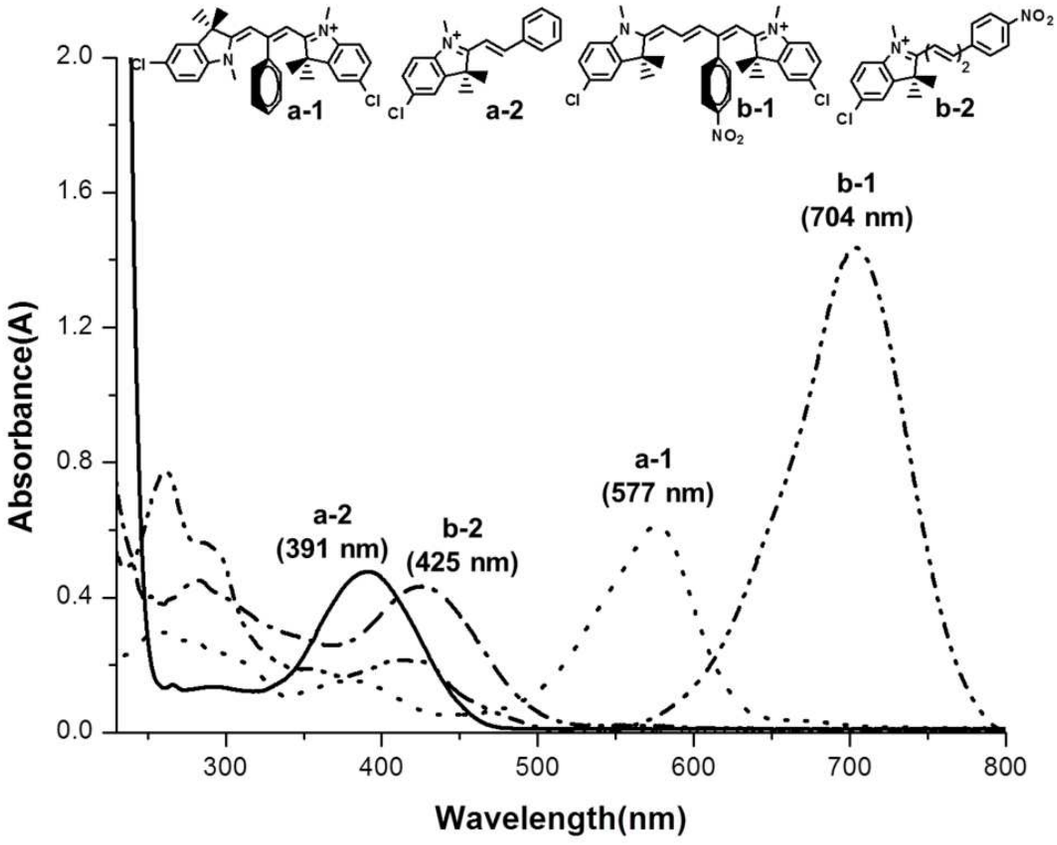

Figure 18. UV-Vis spectral data of LTAM **4** (a) and Un-LTAM **4** (b) in EtOH, showing the various forms such as the TAM+ (a-1 and b-1) and decomposed forms (a-2 and b-2).

Compound[a]	Various structural forms (λ_{max})				
	Leuco- (a)	Carbinol- (b)[b]	TAM+- (c)[c]		Decomposed dye (d)
			x-band	y-band	
Crystal Violet[d]	265	266	585	-	-
Malachite Green[e]	265	265	620	430	-
LTAM **1**	284	343	609	426	385
LTAM **4**	296	327	578	370	391
LTAM **5**	298	-	588	380	390
LTAM **8**	302	363	595	377	318
LTAM **9**	295	-	556	368	382
LTAM **11**	298	-	591	-	403
Un-LTAM **1**	322	381	693	412	420
Un-LTAM **2**	326	383	686	414	415
Un-LTAM **3**	324	368	686	353	435
Un-LTAM **4**	326	384	704	417	425

[a]Names of compounds are the same as in Table 1. [b]The carbinol denoted a hydroxylated TAM+ dye.

[c]Symbols (x-, y-band) are adopted from Ref. (Ernest et al., 1989) [d,e]Data for acetonitrile.

Table 6. UV-Vis spectral data for various forms of LTAM and Un-LTAM compounds.

In the UV-Vis spectral data of Table 6, MG and crystal violet dyes show absorption maxima at 620 and 430 nm for the x- and y-band, respectively, whereas the absorption maxima of the vinyl-log of MG are red-shifted for both the x- and y-bands, *i.e.*, 651 and 488 nm, respectively. This suggests that the vinyl effects of a vinyl unit may, to a large extent, behave like extended conjugation for both the x- and y-bands. Chemical skeletons for the N~N$^+$ and C(phenyl)~N$^+$ responsible for the x- and y-band, respectively, in the absorption spectra of various TAM$^+$ dyes are shown in Fig. 19.

Structurally, the FB analogs of symmetric and unsymmetric TAM$^+$ dyes in this work can be characterized as Cy3 and Cy5 dyes, respectively, as closed-chain cyanines.(Ernst et al., 1989) It was reported that Cy3 is maximally excited at 550 nm and maximally emits at 570 nm in the orange-red part of the spectrum, whereas Cy5 is maximally excited at 649 nm and maximally emits at 670 nm, which is in the red part of the spectrum. Therefore, the x-band of the Un-TAM$^+$ are expected to be higher than 650 nm and 550 nm, for the y- and x-band, respectively.

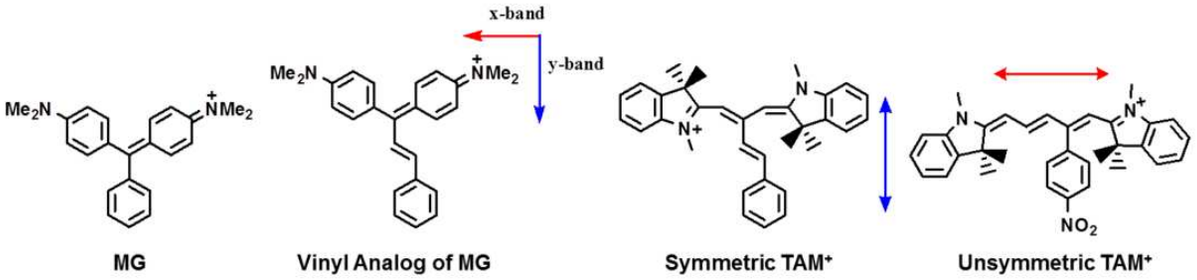

Figure 19. Chemical skeleton for the N~N$^+$ and C(phenyl)~N$^+$ responsible for the x- and y-band, respectively, in the absorption spectra of various TAM$^+$ dyes.

From the reaction of Un-LTAM **4** with $HClO_4$, the decomposed product {5-chloro-1,3,3-trimethyl-2-((1E,3E)-4-(4-nitrophenyl)buta-1,3-dienyl)indolium perchlorate} was isolated, brown, yield 57%, M.p.= 257–258 °C, IR (KBr) 3072, 2984, 2934, 1707, 1596, 1340, and 1086 cm^{-1}, ^{1}H NMR (DMSO-d_6) δ 1.76 (6H, s), 4.03 (3H, s), 7.37 (1H, d, J = 15.3 Hz), 7.66 (1H, dd, J = 10.2, 15.3 Hz), 7.73 (1H, d, J = 9.0 Hz), 7.79 (1H, d, J = 15.3 Hz), 7.92 (2H, d, J = 6.9 Hz), 7.95 (1H, d, J = 9.0 Hz), 8.09 (1H, s), 8.33(1H, dd, (J = 10.2, 15.3 Hz), and 8.33(2H, d, J = 6.9 Hz).

4. Solid state structure

4.1. LTAM molecules

The X-ray crystal structure of LTAM **12,** as a representative example, displays an orthorhombic crystal system with space group *Pna2*$_1$, with a residual factor of $R_1 = 0.0517$. ORTEP diagrams of LTAM **12**, showing atom numbering, are provided in Fig. 20(a).

For LTAM **12**, the C7-C8 and C7-C24 distances are 1.512 and 1.513 Å, respectively, *i.e.*, typical lengths for C-C single bonds, and the enamine C8-C9 and C24-C25 bonds are 1.335 and 1.335 Å, respectively, which are typical lengths for C=C bonds. The LTAM **12** molecules possess three-bladed propeller conformations, similar to earlier reports for various non-

hetaryl LTAM dyes. The inter-plane angles between the aromatic rings A-B, A-C, and B-C in LTAM **12** are 81.29, 87.79 and 86.02°, respectively, as shown in Fig. 20(b).

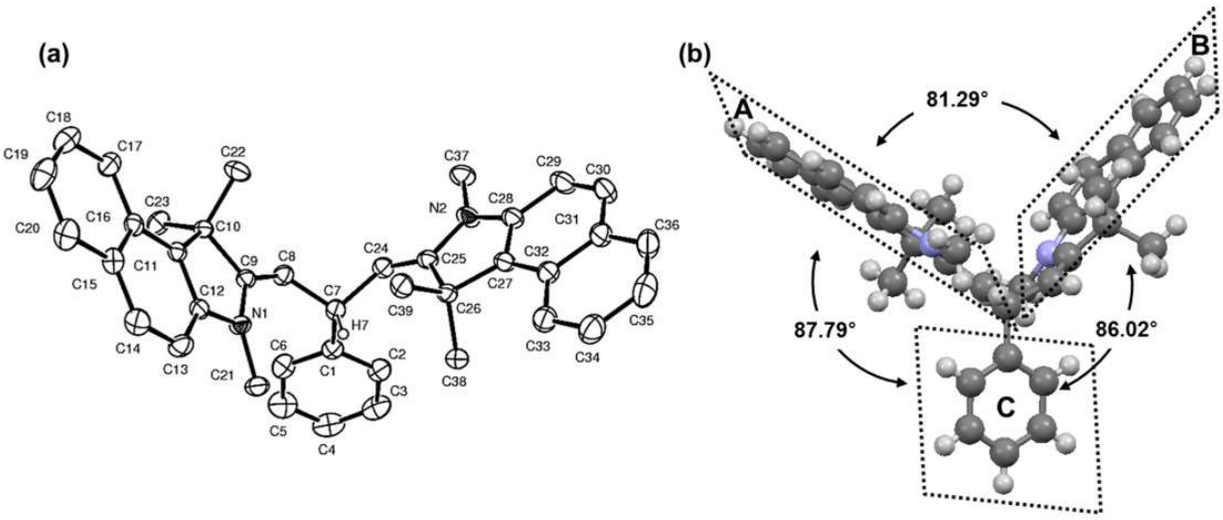

Figure 20. ORTEP diagrams with atom numbering scheme (a) and the propeller shape (b) of LTAM **12**, showing the inter-plane angles.

Selected bond lengths and bond angles for the LTAM molecules are listed in Table 7.

Ring	Bond length (Å) and Bond angle (°)	LTAM molecule			
		4	**5**	**9**	**12**
A	C7-C8	1.513	1.511	1.515	1.512
	C8-C9	1.330	1.341	1.334	1.335
	C9-N1	1.410	1.398	1.400	1.405
	C8-C9-N1	129.42	122.8	129.72	127.47
B	C7-C24	1.507	1.509	1.507	1.513
	C24-C25	1.332	1.334	1.330	1.335
	C25-N2	1.409	1.416	1.407	1.396
	C24-C25-N2	123.06	123.0	123.20	122.94
Others	C7-C8-C9	130.99	128.3	131.06	129.21
	C7-C8-H8	114.5	115.8	114.5	115.4
	C8-C7-H7	107.6	108.6	107.7	112.10
	C7-C24-C25	127.42	129.7	127.68	128.50
	C7-C24-H24	116.3	115.2	116.2	115.8
	C24-C7-H7	107.6	108.6	107.7	107.2

Table 7. Selected bond lengths and bond angles of LTAM molecules.

The dihedral angles H8-C8-C7-H7 and H24-C24-C7-H7 in LTAM **12** are 172.06° (θ_1) and 176.41° (θ_2), respectively. The inter-plane angles and dihedral angles for the LTAM molecules are given in Table 8.

Compound	Interplane angles[a] (º)			Dihedral angles[b] (º)	
	ring A-B	ring B-C	ring A-C	θ_1	θ_2
LTAM **1**	79.8	74.9	84.8	164.1	149.8
LTAM **4**	60.1	75.7	83.2	178.9	158.9
LTAM **7**	77.9	85.6	80.2	152.9	139.8
LTAM **8**	135.4	72.8	72.8	163.2	163.2
LTAM **9**	60.0	77.3	83.5	156.1	179.0
LTAM **11**	44.83	74.32	72.92	174.62	151.68
LTAM **12**	81.29	86.02	87.79	172.06	176.41

[a]Symbols (A-B) and numbering systems are as indicated in Fig. 20(b).
[b]Symbols (θ_1 and θ_2) are the dihedral angles H(8)-C(8)-C(7)-H(7) and H(24)-C(24)-C(7)-H(7), respectively.

Table 8. Inter-plane angles and dihedral angles for LTAM molecules in the solid state.

The C(7)=C(8) double bonds of the two 5-chloro Fischer's base moieties have *EE* configurations in **1**. In contrast, in **2**, the C(14)=C(15) and C(2)=C(3) double bonds of the two 5-chloro Fischer's base moieties belong to the *ZE* configuration. The *EE* (for **1**) and *ZE* (for **2**) isomers formed as the sole product in each case, despite the fact that three isomers, namely *ZE*, *EE*, and *ZZ*, are possible for these dyes which result from the reaction of excess 5-chloro Fischer's base and 4- and 3-pyridine carboxaldehyde.

Compound **12** is stacked so that a dimer is formed in the unit cell of the crystal. The packing in the unit cell of LTAM **12** is distinct, as can be seen in Fig. 21.

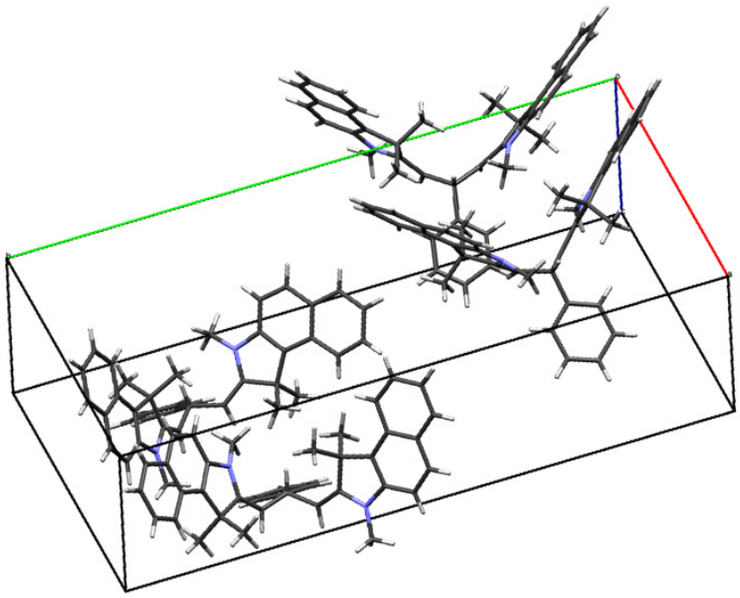

Figure 21. Molecular packing of LTAM **12**, showing the formation of a dimer.

4.2. Un-LTAM molecules

The Un-LTAM **4** was only successfully crystallized from acetone. Unfortunately, crystal growth was unsuccessful for the remainder of the Un-LTAM molecules. Selected bond lengths and bond angles are listed in Table 9.

Ring	Bond length (Å)		Bond angle (°)	
	N1-C2	1.397	C2-N1-C7a	111.7
A	N1-C10	1.439	C2-N1-C10	123.9
	C2-C7''	1.345	C2-C7''-H7''	117.1
	N2-C2'	1.408	C2'-N2-C7a'	111.3
B	N2-C10'	1.445	C7a'-N2-C10'	124.5
	C2'-C11''	1.324	C2'-N2-C10'	123.1
	C1''-C10''	1.516	C9''-C10''-C11''	110.92
	C9''-C10''	1.516	C1''-C10''-C11''	110.01
Conneting group	C10''-C11''	1.509	C9''-C10''-C11''	110.92
	C8''-C9''	1.328	C8''-C9''-C10''	127.29
	C7''-C8''	1.443	C11''-C2'-N2	122.42

Table 9. Selected bond lengths and bond angles of Un-LTAM **4**.

The X-ray crystal structure of Un-LTAM **4** shows a triclinic crystal system with space group *P-1*. An ORTEP diagram of Un-LTAM **4**, including the atom-numbering scheme, is shown in Fig. 22(a).

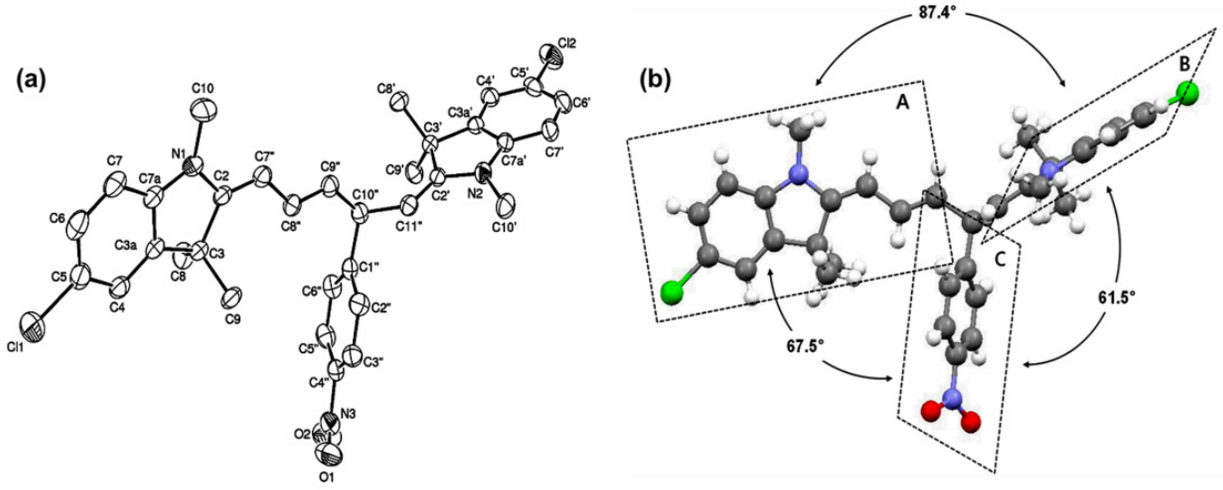

Figure 22. ORTEP diagrams with atom numbering scheme (a) and the propeller shape (b) of Un-LTAM **4**, showing the inter-plane angles.

The C9''-C10'' and C10''-C11''' distances are 1.516 and 1.509 Å, respectively, typical for C–C single bonds. The C7''-C8'' single bond distance, however, was 1.443 Å, which is shorter than a typical single bond and longer than a typical double bond. This is perhaps due to conjugation since the length (1.47 Å) of the central single bond of 1,3-butadiene is approximately 6 ppm shorter than that of the analogous single bond (1.53 Å) in butane. The two enamine C2=C7'' and C2'=C11'', and C8''=C9'' double bonds were 1.354, 1.324, and 1.328 Å, respectively, which are typical C=C bond lengths. In the crystal, the three aromatic rings of **4** are linked to three different layers, *viz.* a vinyl FB, a FB, and a phenyl group. The unsymmetrical molecule is a distorted version of the well-known three-bladed propeller conformation. (Keum et al., 2011). The inter-plane angles of the aromatic rings A–B, A–C, and B–C in Un-LTAM **4** are 87.4°, 67.5°, and 61.5°, respectively (Fig. 22(b)).

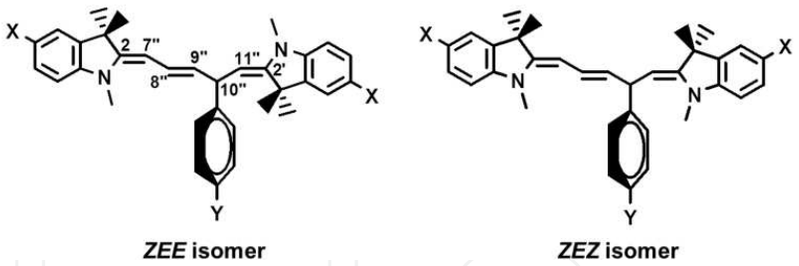

Figure 23. Chemical structures of Un-LTAM , with *ZEE* and *ZEZ* configurations.

The double bonds C2=C7'', C8''=C9'', and C2'=C11'' of Un-LTAM **4** have *EEE* configurations. The *EEE* isomers of these LTAM dyes are formed as the sole product in all cases, even though there are three possible isomers, the two other diastereomers being the *ZEE* and *ZEZ* isomers, as shown in Fig. 23. Generally, the central carbon-carbon double bond of these LTAM dyes is expected to have an *E* configuration.

Although the presence of the *ZEE* and *ZEZ* diastereomers was generally expected to be found in organic solvents, none of these isomers were detected, unlike for the LTAM molecules examined previously.

Fig. 24 shows the molecular packing diagram of Un-LTAM **4**, showing the formation of the dimer, which is stacked in an alternating fashion in the unit cell of the crystal. The intermolecular distances in the dimer are 8.53 and 9.40 Å, for the FB and phenyl rings, respectively.

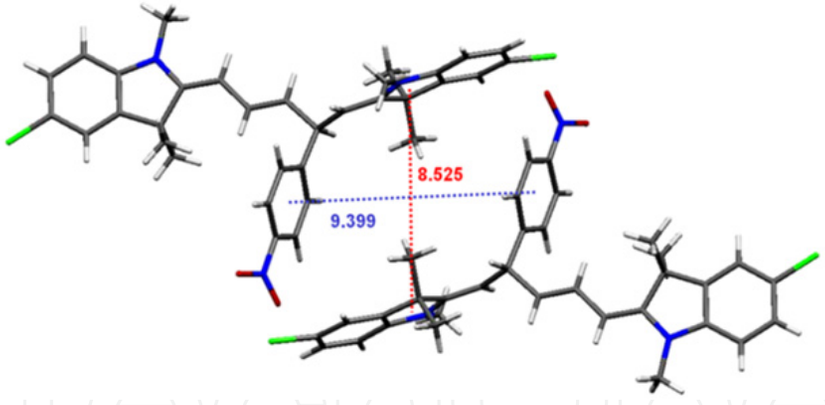

Figure 24. Molecular packing diagram of Un-LTAM **4**, showing formation of the dimer.

5. Conclusion

Novel Fischer's base analogs of LTAM and Un-LTAM molecules and their corresponding TAM^+ dyes have been successfully developed. ^1H and ^{13}C NMR assignments for the prepared LTAM molecules have been completed by 1D and 2D NMR experiments, including DEPT, COSY, HSQC, HMBC, and NOESY. The geometry of the double bond was *ZE* in most cases, as measured directly by NOESY. The *EE* and *ZZ* isomers have C_2 symmetry, and hence, the two FB rings of these isomers are identical. Therefore, the ^1H NMR spectra of the *EE* and *ZZ* isomers are expected to be relatively simple compared to those of the *ZE* isomer. The novel LTAM molecules exist as a single isomer (*ZE* or *EE*) in the

solid phase and they are equilibrated with other isomers in organic solvents. The percent ratios among the diastereomeric isomers of LTAM derivatives in the thermal equilibrium states vary according to the molecules examined and solvents used.

UV-Vis spectral data shows various structural forms of the LTAM and Un-LTAM molecules, such as (a) leuco-, (b) colored TAM^+, (c) carbinol-, and (d) decomposed-forms, similar to the commercially known TAM^+ dyes, such as MG, crystal violet, etc. Particularly, UV-Vis spectroscopic data for the Un-TAM^+ dyes showed absorptions in the near-IR region.

X-ray crystal analysis showed that the *ZE* isomers were generally formed with a so-called three-bladed propeller conformation. These isomers stacked to form a dimer or double dimer. However, the *EE* isomers were also formed specifically for the LTAMs **3**, **5**, **8**, and **11**, which have a resonance-electron withdrawing (-R) group at the para-position of the phenyl ring. Further analysis of a variety of substituted LTAM molecules is required to determine what makes the diastereomer structures change in the solid state.

Author details

Sam-Rok Keum, So-Young Ma and Se-Jung Roh
Korea University at Sejong Campus, South Korea

Acknowledgement

This research was supported by Basic Science Research Program through the National Research Foundation of Korea (NRF) funded by the Ministry of Education, Science and Technology (No.2012003244) and partly by the Brain Korea 21 project.

6. References

Anslyn, E.V. & Dougherty, D.A. (2006). *Modern Physical Organic Chemistry*, University Science Books, U.S. pp. 365-367.

Balko L, Allison J. The direct detection and identification of staining dyes from security inks in the presence of other colorants, on currency and fabrics, by laser desorption mass spectrometry. *J. Foren. Sci.* 2003, *48*: 1172–8.

Bartholome, D. & Klemm, E. (2006). Novel Polyarylene−Triarylmethane Dye Copolymers, *Macromolecules*, Vol. 39 pp. 5646-5651.

Cho BP, Yang T, Lonnie R, Blankenship L, Moody JD, Churchwell M, Beland FA. Culp S. *J. Chem. Res. Toxicol.* 2003, *19*, 285.

Ernst, L. A.; Gupta, R. K,; Mujumdar, R. B. & Waggoner, A. S. (1989). Cyanine dye labeling reagents for sulfhydryl groups, *Cytometry* Vol. 10, pp. 3-10.

Fengling, S. F. & Xiaojun, P. X. (2005). Heptamethine Cyanine Dyes with a Large Stokes Shift and Strong Fluorescence: A Paradigm Excited-State Intramolecular Charge Transfer. 2. *J. Am. Chem. Soc.* Vol. 127, pp. 4170-4171.

Gessner, T. & Mayer, U. (2005). Triarylmethane and Diarylmethane Dyes, *Ullmann's Encyclopedia of Industrial Chemistry*, Weinheim: Wiley-VCH, doi:10.1002/14356007.a27-179

Indig GL, Anderson GS, Nichols MG, Bartlett JA, Mellon WS, Sieber F. Effect of molecular structure on the performance of triarylmethane dyes as therapeutic agents for photochemical purging of autologous bone marrow grafts from residual tumor cells. *J. Pharm. Sci.* 2000, *89*: 88–99.

Kraus, G. A.; Jeon, I.; Nilsen-Hamilton, M.; Awad, A. M.; Banerjee J. & Parvin, B. (2008). Fluorinated Analogs of Malachite Green: Synthesis and Toxicity, *Molecules*, Vol. 13, No. 4, pp. 986-994; doi:10.3390/molecules13040986

Keum, S. R.; Roh, S. J,; Lee, M. H.; Saurial, F. & Buncel, E. (2008). ^{1}H and ^{13}C NMR assignments for new heterocyclic TAM leuco dyes, (2*Z*,2′*E*)-2,2′-(2-phenyl propane-1,3-diylidene)bis(1,3,3-trimethylindoline) derivatives. Part II. *Magn. Reson. Chem*. Vol. 46, pp. 872–877.

Keum, S. R.; Roh, S. J.; Kim, Y.N.; Im, D.H. & Ma, S. Y. (2009). X-ray crystal structure of hetaryl leuco-TAM dyes, (2Z,2′*E*)-2,2′-(2-phenylpropane-1,3-diylidene) bis(1,3,3-trimethyl indoline) derivatives. *Bull. Korean Chem. Soc*. Vol. 30, pp. 2608–2612.

Keum, S. R.; Roh, S. J,; Ma, S. Y.; Kim, D. K. & Cho, A. E. (2010). Diastereomeric isomerization of hetaryl leuco-TAM dyes, (2Z, 2′E)-2,2′-(2-phenyl propane-1,3-diylidene) bis(1,3,3-trimethylindoline) derivatives in various organic solvents. *Tetrahedron*, Vol. 66, pp. 8101–8107.

Keum, S. R.; Lee, M. H.; Ma, S. Y.; Kim, D. K. & Roh, S. J. (2011). Novel unsymmetrical leuco-TAM, (2*E*, 2′*E*)-2,2′-{(E)-4-phenylpent-2-ene-1,5-diylidene}bis(1,3,3-trimethyl indoline) derivatives: synthesis and structural elucidation. *Dyes and Pigments*, Vol. 90, pp. 233–238.

Liao, S. & Collum, D. B. (2003). Lithium Diisopropylamide-Mediated Lithiations of Imines: Insights into Highly Structure-Dependent Rates and Selectivities, *J. Am. Chem. Soc.* Vol. 125, pp. 15114-15127.

Li, Z.; Duan, Z.; Kang, J.; Wang, H.; Yu, L. & Wu, Y. (2008). A simple access to triarylmethane derivatives from aromatic aldehydes and electron-rich arenes catalyzed by $FeCl_3$, *Tetrahedron* Vol. 64, pp. 1924-1930.

Ma, S. Y.; Kim, D. K.; Lim, H. Y.; Roh, S. J. & Keum, S. R. (2012). Unusual Stability of Diastereomers of the Isomeric Pyridine-based Leuco-TAM Dyes 2,2'-(2-(Pyridin-4 or 3-yl) propane-1,3-diylidene)bis(5-chloro-1,3,3-trimethylindoline), *Bull. Korean Chem. Soc.* Vol. 33, pp. 681-684.

Nair, V.; Thomas, S.; Mathew, S. C. & Abhilash, K. G. (2006). Recent advances in the chemistry of triaryl- and triheteroarylmethanes. *Tetrahedron*, Vol. 62, pp. 6731-6747.

Özer, I. & Çaglar, A. (2002). Protein-mediated nonphotochemical bleaching of malachite green in aqueous solution. *Dyes & Pigments*, Vol. 54, pp. 11-16.

Plakas, S. M.; Doerge, D. R.; Turnipseed, S. B. In Xenobiotics in Fish; Kluwer Academic and Plenum Publisher: NY. 1999; pp. 149.

Keum, S. R.; Ma, S. Y.; Kim, D. K.; Lim, H. W. & Roh, S. J. (2012). Novel dimeric leuco-TAM dyes, 1,4-bis{(1*E*,3*Z*)-1,3-bis(1,3,3-trimethylindolin-2-ylidene)propan-2-yl}benzene derivatives: Structure and spectroscopic charactierization. *Journal of Molecular structure*, Vol. 1014, pp. 25-32.

Keum, S. R.; Ma, S. Y.; Kim, D. K.; Lim, H. W. & Roh, S. J. (2012). Unsymmetric leuco-TAM dyes, (2*E*, 2′*E*)-2,2′-{(E)-4-phenylpent-2-ene-1,5-diylidene}bis(1,3,3-trimethylindoline) derivatives. Part II: X-ray crystal structure☆. *Dyes and Pigments*, Vol. 94, pp. 490–495.